Research in Astronomy and Astrophysics, 22:105012 (12pp), 2022 October https://doi.org/10.1088/1674-4527/ac8d81

Wiener Filtration Algorithm of an Ensemble Pulsar Timescale Based on a Power-law Model of Pulsar Power Spectrum

Ting-Gao Yang[1,2], Ming-Lei Tong[1,2,3], and Yu-Ping Gao[1,2,3]
[1] National Time Service Center, Chinese Academy of Sciences, Xi'an 710600, China; mltong@ntsc.ac.cn
[2] Key Laboratory of Time and Frequency Primary Standards, Chinese Academy of Sciences, Xi'an 710600, China
[3] University of Chinese Academy of Sciences, Beijing 100049, China
Received 2022 May 27; revised 2022 August 8; accepted 2022 August 23; published 2022 October 4

Abstract

An ensemble pulsar timescale derived from the traditional Wiener filtration still contains some high level noise. To improve this situation we developed a Wiener filtration algorithm of the ensemble pulsar timescale based on a power-law model of power spectrum for pulsars. Our algorithm has three strengths: (1) mitigating spectral leakage between frequency bins for Fourier techniques; (2) using a power-law model for power spectrum; (3) signal realization in original residuals of data set by the power-law model. According to improved algorithm we constructed an ensemble pulsar timescale EPT−TAI using timing data with respect to International Atomic Time (TAI) about 16 yr time span of ten pulsars from International Pulsar Timing Array second data release (version A). The results show that EPT−TAI detected correctly the differences TT(BIPM2015)−TAI between terrestrial time TT(BIPM2015) and TAI. Fractional frequency stability σ_z analysis shows that EPT−TAI does not indicate red noise for 16 yr time interval, and fractional frequency stability for 8 yr and longer time intervals is slightly better than that of TT(BIPM2015)−TAI. Stability for short time intervals of TT(BIPM2015)−TAI is better than that of EPT−TAI, but TT(BIPM2015)−TAI shows red noise for longer time intervals. Using the same algorithm we also derived an ensemble pulsar timescale EPT−TT(BIPM2015) with respect to TT(BIPM2015). The fractional frequency stability curve of EPT−TT(BIPM2015) shows similar characteristics as that of EPT−TAI but with slightly lower values.

Key words: (stars:) pulsars: general – time – methods: data analysis

1. Introduction

International Atomic Time (TAI) is the basic timescale kept by the Bureau International des Poids et Mesures (BIPM) using time keeping data of atomic clocks over the world. In order to further improve TAI (Guinot 1988), BIPM developed terrestrial time TT(BIPMXXXX) where XXXX indicates publishing year. For convenience in the following text, TT also denotes terrestrial time, and TT−TAI is quadratically fitted timescale in order to make comparison with pulsar timescale.

Atomic time is the integrated timescale based on atomic clocks. Pulsar time based on rotation phase of millisecond pulsars is entirely different from atomic time by their physical mechanisms. Pulsar timescale can supply a valuable independent check on atomic time. An ensemble pulsar timescale can be constructed using long term timing data of millisecond pulsars. Rodin (2008) introduced Wiener filtration algorithm for constructing an ensemble pulsar timescale and showed result using early timing data of two pulsars. Hobbs et al. (2012), Hobbs et al. (2020) described generalized least square fitting and Bayesian analysis methods for ensemble pulsar timescale and have shown that developed ensemble pulsar timescale correctly detected errors of TAI. Long term stability of ensemble pulsar timescale is comparable to that of atomic timescale. Today, the International Pulsar Timing Array (IPTA) (Manchester et al. 2007; Hobbs et al. 2010; Manchester 2011; Hobbs 2012) has obtained long term timing data for more than 60 ms pulsars. Among them there are about 20 yr long continuous timing data available for some pulsars. IPTA timing data for 49 ms pulsars were released in 2016 (Verbiest et al. 2016) and timing data for 65 pulsars were released in 2019 for the second data release (Perera et al. 2019).

Time of arrival (TOA) of electromagnetic radiation from pulsars can be measured by radio telescopes in reference to an atomic timescale, for example TAI or TT. Transformation between measured TOAs and the times of radiation from pulsars is described by a timing model (Edwards et al. 2006). The timing model characterizes astrometric properties of the observed pulsar, such as position and proper motion as well as its timing properties such as spin period, and additional orbital parameters if the pulsar is in a binary. Dispersion measure (DM) and possible variation of the interstellar and planetary medium must be measured. For timing data analysis an accurate ephemeris of solar system objects is used.

For any pulsar, we adopt a model for the observed TOAs which we denote $\boldsymbol{d}$, that results from a number of contributions and physical effects according to

$$\boldsymbol{d} = \boldsymbol{\tau}^{\mathrm{TM}} + \boldsymbol{\tau}^{\mathrm{WN}} + \boldsymbol{\tau}^{\mathrm{RN}} + \boldsymbol{\tau}^{\mathrm{DM}} + \boldsymbol{\tau}^{\mathrm{CLK}} + \boldsymbol{\tau}^{\mathrm{EPH}} + \boldsymbol{\tau}^{\mathrm{GW}}. \quad (1)$$

In Equation (1) (Lentati et al. 2015), $\boldsymbol{\tau}^{\mathrm{TM}}$ represents the deterministic timing model, which can be fitted by joint analysis including the timing model and noise model parameters. $\boldsymbol{\tau}^{\mathrm{WN}}$ denotes white noise of pulsar timing which is stochastic contribution due to the combination of instrument thermal noise and intrinsic pulsar white noise. The original measured errors of TOAs must be modeled and corrected. $\boldsymbol{\tau}^{\mathrm{RN}}$ is stochastic contribution due to red spin noise which can be estimated by a power-law model of power spectrum. $\boldsymbol{\tau}^{\mathrm{DM}}$ is stochastic contribution due to changes in the dispersion of radio pulses traveling through the interstellar and interplanetary medium. $\boldsymbol{\tau}^{\mathrm{DM}}$ can be measured by multi-frequency observations (Keith et al. 2013; Lee et al. 2014). These four terms above depends on the pulsar, but they are independent across pulsars included in a timing array. $\boldsymbol{\tau}^{\mathrm{CLK}}$, $\boldsymbol{\tau}^{\mathrm{EPH}}$ and $\boldsymbol{\tau}^{\mathrm{GW}}$ represent respectively stochastic contributions from clock signal, errors in a solar system ephemeris used and a gravitational wave. These three terms belong to "common noise" present across all pulsars in a timing array, but they have distinguishable characteristics due to their different correlation across pulsars in an array.

Our purpose is to construct an ensemble pulsar timescale, in other words, we hope to extract clock signal from a long term timing data set of pulsars in a timing array. So we must accurately determine timing model parameters for each pulsar in the data set used, remove any systematic errors dependent on observational system or DM variation, and mitigate other stochastic contributions such as red spin noise and possible noises from solar system ephemeris and gravitational waves. The key technique of constructing an ensemble pulsar timescale is about design on a suitable algorithm employed. Traditional Wiener filtration can be used, but the ensemble pulsar timescale derived usually contains some high level noise. It is still not convenient to extract clock signal from residuals of pulsars in an array by Wiener filtration. To improve this situation we developed a Wiener filtration algorithm based on a power-law model of pulsar power spectrum.

In Section 2, we describe data set used to construct an ensemble pulsar timescale. In Section 3, we introduce the traditional Wiener filtration algorithm and show results of analysis by this method. In Section 4, a detailed description on the improved Wiener filtration algorithm is given. An ensemble pulsar timescale computed by our improved algorithm is shown. Fractional frequency stability for timescales are analyzed. Finally in Section 5, some discussions and conclusions are provided.

Table 1
General Characteristics of Timing Data with Common Period from MJD 50,639 to MJD 56,759 for Ten Pulsars from IPTA Second Data Release (Version A)

Pulsar Name	Pulse Period (ms)	rms of Residuals with Respect to TAI(μs)	Number of TOAs	Weight (EPT1−TAI)	Weight (EPT−TAI)
J0437-4715	5.757	0.166	4598	0.5952	0.2238
J0751+1807	3.479	2.419	1491	0.0015	0.0026
J1012+5307	5.256	1.404	7266	0.0024	0.0001
J1022+1001	16.453	2.158	1256	0.0301	0.0015
J1640+2224	3.163	1.877	2451	0.0067	0.0004
J1713+0747	4.570	0.256	12 242	0.3294	0.5618
J1730-2304	8.123	2.277	566	0.0094	0.0123
J1744-1134	4.075	0.689	5217	0.0169	0.1839
J2124-3358	4.931	3.080	1103	0.0070	0.0066
J2145-0750	16.052	1.707	4525	0.0013	0.0071

Note. The last two columns show normalized weight of each pulsar for constructing ensemble pulsar timescale EPT1−TAI and EPT−TAI respectively (see Section 4.2).

2. The Data Set Used

Initial TOA data series for ten pulsars with longest time span in the same period were selected from the IPTA second data release (version A)[4] (Perera et al. 2019). Considering the effect of possible DM error on the data, the observations below 1000 MHz were removed. So selected TOA data set for the ten pulsars covers a period from MJD 50,639 to MJD 56,759. In this period the largest spacing between any adjacent two initial TOA points is less than 390 days for any pulsar in the selected data set. The general characteristics for the selected ten pulsars are given in Table 1. The rotation period, rms of post-fit residuals and total number of TOAs in the selected common period for each pulsar some are shown in Table 1. Post-fit residuals with respect to TAI and to TT(BIPM2015) were formed respectively for each pulsar in the selected data set using TEMPO2.[5] We will use post-fit residuals with respect to TAI to calculate an ensemble pulsar timescale EPT−TAI. Similarly an ensemble pulsar timescale EPT−TT(NIPM2015) will be computed using post-fit residuals with respect to TT(BIPM2015). For satisfying requirements of the Wiener filtration algorithm, we further process the post-fit residuals of each pulsar in the data set as follows:

(1) Combining data points of residuals with the same MJD and then rearranging the residual series in order according to corresponding MJDs.

(2) Removing data points with absolute value of residual larger than three times of the rms of residuals.

(3) Making moving average (Petit & Tavella 1996) of residual series to obtain average data points with equal spacing

[4] http://www.ipta4gw.org
[5] https://bitbucket.org/psrsoft/tempo2

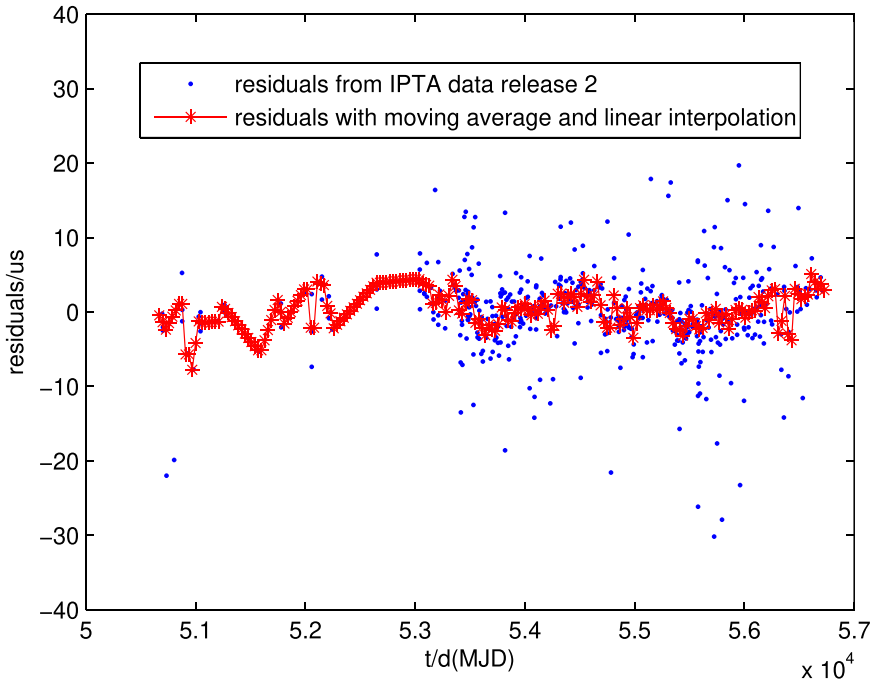

Figure 1. Timing residuals with respect to TAI of pulsar J1730-2304 which has sparsest TOA distribution in the ten pulsar data set. The blue points represent initial residual series with the data below 1000 MHz observations removed. Red * represents equal spacing data points after removing outliers, moving average and linear interpolation.

of 30 days. Each average data point of residuals is computed within a time interval of 60 days. Corresponding MJD of the middle point of the first 60 days interval is taken as MJD of the first average point. Then the second average data point is computed within 60 days interval with the current and next 30 days data, and so on.

(4) If no observational data are available in any 60 days time interval, linear interpolation between two adjacent data points available from data computed by moving average is implemented to make up absent data points. For example, because of missing observations of TOA data especially for the early period of pulsar J1730-2304, there are several time intervals about 1 yr with no data available. Figure 1 shows distribution of residuals for J1730-2304. Blue points represent initial post-fit residuals with observations below 1000 MHz removed. The red curve indicates equal spacing data points after removing outliers, moving average and linear interpolation. Since the clock signal that we concerned consists of low frequency components, moving average and linear interpolation perturb high frequency components but leave low frequency signal (Petit & Tavella 1996; Rodin 2008).

Finally the equal spacing residual series with sample interval 30 days and 203 data points for each pulsar are quadratically refitted for consistency with the classical timing fitting.

3. Wiener Filtration Algorithm and Results

3.1. Wiener Filtration Algorithm

Wiener filtration has been used for pulsar timing data analysis for a long time. For example, when a signal concerned in timing residuals was modeled and model parameters were properly determined, then signal waveform can be constructed by Wiener filter (Lee et al. 2014; Hobbs et al. 2020). This usage of Wiener filter is extended to irregular spacing data set. For constructing an ensemble pulsar timescale by Wiener filtration, post-fit timing residuals of each pulsar in the data set selected are required and correctly formed by Tempo2 package. Through further processing one acquires the same equal spacing data set of the post-fit residuals for all pulsars in the data set. We denote the equal spacing data for each pulsar as vector $\boldsymbol{r}_I$, where subscript I indicates the Ith pulsar. $\boldsymbol{r}_I$ usually contains clock signal, timing noise and other possible stochastic noises such as gravitational wave and errors of the used ephemeris of solar system bodies. Assuming that $\boldsymbol{Q}_{ss}$ is covariance matrix of the clock signal interested in, $\boldsymbol{Q}_{rI}$ is covariance matrix of the vector $\boldsymbol{r}_I$ and w_I is normalized weight for the pulsar I, if the number of pulsars is n, the optimal estimator for the clock signal can be written as (Zhong & Yang 2007; Rodin 2008)

$$\hat{\boldsymbol{s}} = \boldsymbol{Q}_{ss}\sum_{I=1}^{n}(w_I\boldsymbol{Q}_{rI}^{-1}\boldsymbol{r}_I). \quad (2)$$

The key technique for the Wiener filtration is how to form covariance matrix $\boldsymbol{Q}_{rI}$ and $\boldsymbol{Q}_{ss}$. First we calculate covariance function, then covariance matrix is easily formed by covariance function. The clock signal concerned has the same correlation with each pulsar in the data set selected. Obviously at least two or more pulsars are needed to calculate covariance function for clock signal. For n pulsars, the number of the independent pair of pulsars that can be formed is m, where $m = n(n-1)/2$. We calculate their respective cross-power spectrum using post-fit residuals $\boldsymbol{r}_I$ and $\boldsymbol{r}_K (I \neq K)$ and then cross-covariance function is derived for each pair of pulsars. Finally we take the average cross-covariance function of all the pairs of pulsars as estimated covariance function for the clock signal. Because their timing noise for the different pulsars are independent, the average cross-covariance function can better remove the effect of timing noise and also mitigate other possible disturbing noises. Similar auto-covariance function for each pulsar can be calculated from their respective vector $\boldsymbol{r}_I$ of the post-fit residuals.

For calculation of auto- and cross-covariance functions the following algorithm (Rodin 2008) is used. Rewriting vector $\boldsymbol{r}_I$ as $\boldsymbol{r}_{I,t}$, where I is the index of pulsars as before, and t is the index of data points in the vector. If N is length of the vector $\boldsymbol{r}_{I,t}$, Fourier transformation for the pulsar I is given by

$$x_I(\varpi) = \sum_{t=1}^{N} (\boldsymbol{r}_{I,t} \boldsymbol{h}_t e^{-j\varpi t}), \tag{3}$$

where $\boldsymbol{h}_t$ is smoothing window function used to mitigate spectral leakage problem (Rodin 2008). The auto-power spectrum ($I = K$) and the cross-power spectrum ($I \neq K$) for the data set of pulsars used to construct an ensemble pulsar timescale are calculated from the formula

$$X_{I,K}(\varpi) = |x_I(\varpi) x_K^*(\varpi)|. \tag{4}$$

In formula (4), $(.)^*$ indicates complex conjugation. The auto-covariance function ($I = K$) and the cross-covariance ($I \neq K$) are calculated by the formula

$$\mathrm{cov}(r_I, r_K) = \sum_{\varpi=1}^{N} X_{I,K}(\varpi) e^{j\varpi t}. \tag{5}$$

3.2. Results

Figure 2 shows the ensemble pulsar timescale EPT1−TAI (blue curve) derived by Wiener filtration method introduced above using the data set with ten pulsars described in Section 2. The red curve is the clock signal TT(BIPM2015)−TAI. Clearly the EPT1−TAI contains much noise. In order to separate the clock signal from the EPT1−TAI, we need to design a suitable filter to further filter out clock signal from noisy EPT1−TAI data.

4. Wiener Filtration Algorithm Based on a Power-law Model of Power Spectrum and Results

4.1. Description of the Algorithm

The Wiener filtration algorithm based on a power-law model of power spectrum is an improved algorithm of the traditional Wiener filtration. We improve the Wiener filtration algorithm for ensemble pulsar timescale following three aspects.

(1) Mitigating spectral leakage between frequency bins for Fourier techniques

For the Wiener filtration method both auto-power spectrum and cross-power spectrum of pulsar residuals are based on Fourier techniques. In order to effectively mitigate spectral leakage between frequency bins for Fourier techniques, power spectrum is analyzed with "pre-whitening" and "post-darkening" (Coles et al. 2011). One applies a linear pre-whitening filter which is implemented in the time domain. If $x(k)$ is the input residuals and $y(k)$ is the output, a first difference is $y(k) = x(k+1) - x(k)$. Fourier transformation for the whitened data $y(k)$ is implemented. We then correct the estimated spectrum of the whitened data by dividing it by $|2\sin(\pi f \delta)|^2$, where f is Fourier frequency and δ is the sample time interval of residuals $x(k)$. Figure 3 shows power spectrum for the atomic timescale TT(BIPM2015)−TAI. In Figure 3, the black curve is the result from Fourier transformation according to Equation (3), where smoothing window function $\boldsymbol{h}_t$ is calculated by formula (9) in Rodin (2008). The red curve is result from analyzing with "pre-whitening" and "post-darkening" (Coles et al. 2011). In Figure 3 one can see that the black curve is still affected by spectral leakage into the high frequency components of Fourier techniques, the red curve effectively mitigated spectral leakage problem. From Figure 3 we can also conclude that power spectrum of the TT(BIPM2015)−TAI is better described by a power-law model.

(2) Using a power-law model for power spectrum

Auto-power spectrum of residuals for each pulsar contain timing noise and clock signals. The common clock signal can be extracted through cross-power spectrum of pulsar pair. So cross-power spectrum is considered as power spectrum of the clock signal. Because timing noise depends only on the pulsar, for different pulsars, their timing noises are independent. Timing noise may be mitigated through cross-power spectrum of pulsar pair. Auto-power spectrum of pulsar $S_{\mathrm{auto}}(f)$ and cross-power spectrum of pulsar pair $S_{\mathrm{clk}}(f)$ can be respectively described using a power-law model (van Haasteren & Levin 2009; Coles et al. 2011; Lentati et al. 2013; van Haasteren et al. 2013; Lentati et al. 2014; Caballero et al. 2016; Hobbs et al. 2020) as follows:

$$S_{\mathrm{auto}}(f) = S_{0,\mathrm{auto}} \left(\frac{f}{1\ \mathrm{yr}^{-1}} \right)^{\alpha_{\mathrm{auto}}}, \tag{6}$$

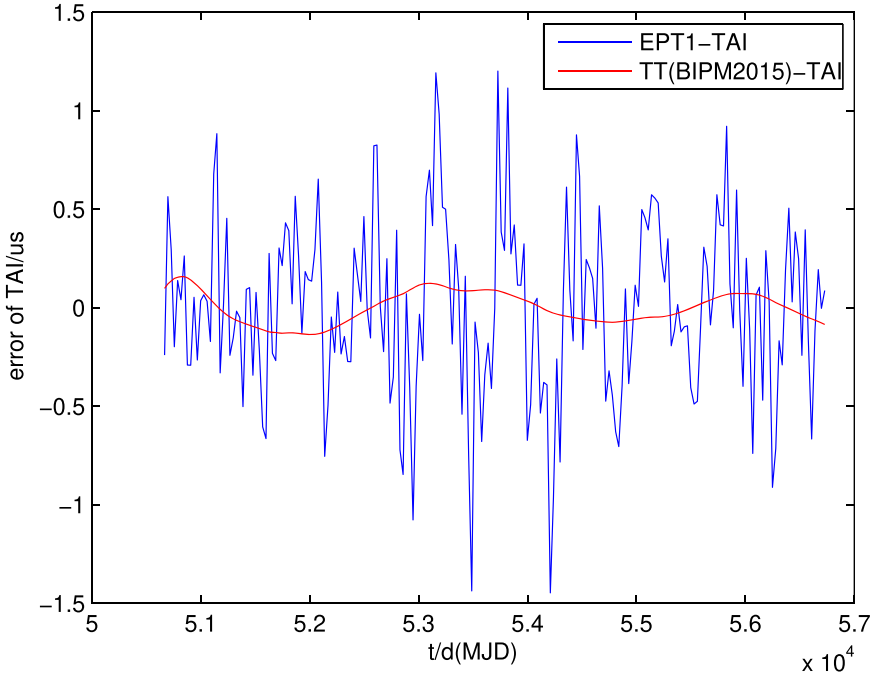

Figure 2. Ensemble pulsar time EPT1−TAI (blue curve) and signal of TT(BIPM2015)−TAI (red curve). EPT1−TAI shows some high level noise.

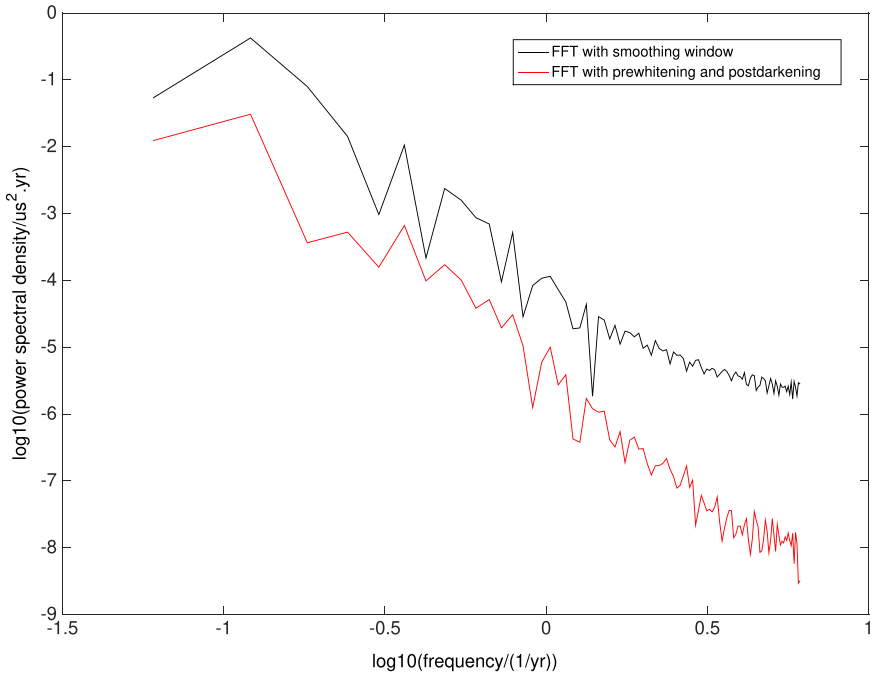

Figure 3. Power spectrum of TT(BIPM2015)−TAI. The black curve is derived using Fourier transformation with a smoothing window. The effect of spectral leakage into high frequencies is observed. The red curve is analyzed using "pre-whitening" and "post-darkening" methods.

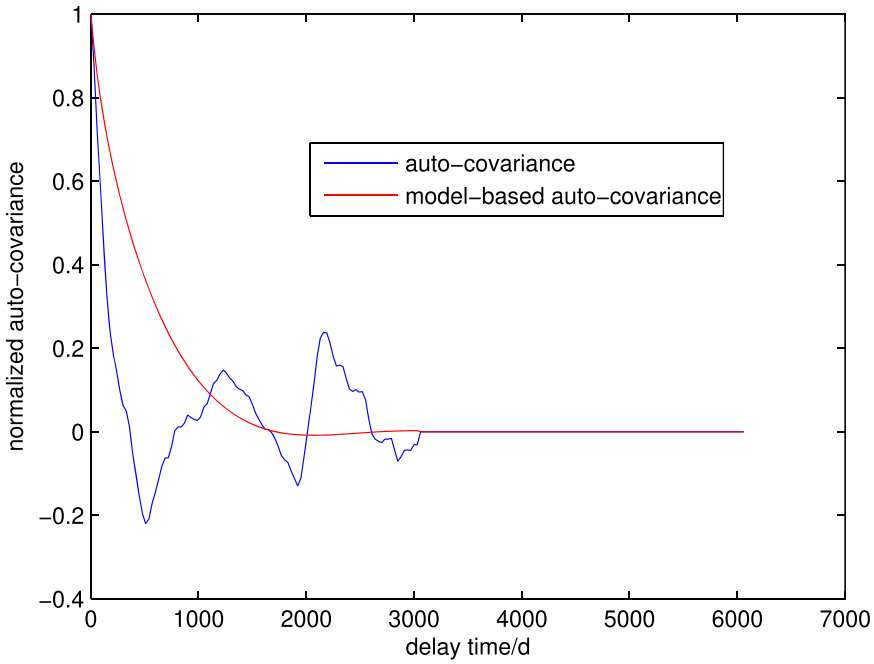

Figure 4. Normalized auto-covariance function of J0437-4715. The blue curve is derived from the auto-power spectrum of the residuals with respect to TAI. The red curve is derived from the auto-power spectrum based on a power-law model. The blue curve converges to the red one.

where $S_{0,\mathrm{auto}}$ is the amplitude of auto-power spectrum of frequency $1\mathrm{yr}^{-1}$, α_{auto} is the index of the auto-power spectrum.

$$S_{\mathrm{clk}}(f) = S_{0,\mathrm{clk}}\left(\frac{f}{1\ \mathrm{yr}^{-1}}\right)^{\alpha_{\mathrm{clk}}}, \tag{7}$$

where $S_{0,\mathrm{clk}}$ is the amplitude of cross-power spectrum of frequency $1\ \mathrm{yr}^{-1}$, α_{clk} is the index of the cross-power spectrum. In order to correctly derive power-law model parameters for both auto- and cross-power spectrum, power-law model fitting in logarithmic space is based on the Fourier lower frequency components of relative power spectrum.

Parameters of power-law model of the auto-power spectrum for each pulsar are fitted to its auto-power spectrum. Then the auto-power spectrum is reconstructed by its model parameters. The auto-covariance function of each pulsar is calculated using the reconstructed auto-power spectrum by following equation (Hobbs et al. 2020)

$$C_{t_{ij}}^{\mathrm{auto}} = \int_{1/T}^{f_c} S_{\mathrm{auto}}(f)\cos(2\pi f t_{ij})df, \tag{8}$$

In Equation (8) T is the total time span for pulsar residuals in the data set, $1/T$ is the frequency of lower-limit of integration, because the signal with frequency lower than $1/T$ was absorbed by a quadratic spin model fitting. f_c is the frequency of up-limit of integration, the ij indices denote the time epochs and t_{ij} is the time lag between the two respective epochs. Normalized auto-covariance function for the pulsar J0437-4715 is shown in Figure 4. In Figure 4, the red curve is auto-covariance function based on the power-law model. The blue one denotes auto-covariance function calculated directly using the auto-power spectrum of the residuals. The blue curve converges to the red one for the high frequency covariance. The similarly normalized auto-covariance function for J0715+1807 is shown in Figure 5.

To insure auto-covariance function of each pulsar is correctly derived, we show a brief comparison between our power-law model parameter of auto-power spectrum and a published result which is derived by the Bayesian method. The spectral indices we derived for J0437-4715, J1713+0747 and J1744-1134 are respectively −1.6, −1.3 and −1.1; their Bayesian result is about −1.8, −1.4 and −1.2 which is approximately estimated from Figure 3 of Hobbs et al. (2020). The two results are compatible although their data set is not exactly the same. Above three pulsars take very large weight for computation of an ensemble pulsar timescale (see Table 1, also see Table 1 of Hobbs et al. (2020)). Since the scale of our power spectrum is different from Hobbs et al. (2020) the amplitude of the power-law model of auto-power spectrum is not shown. If auto-power spectral model parameters for each pulsar are determined by the Bayesian analysis, they can be used for auto-covariance calculation.

By fitting a power-law model to the cross-power spectrum for each independent pulsar pair in the data set, we obtain its power-law model parameters. The power-law model of cross-power spectrum is denoted by Equation (7). Using the model parameters obtained above we reconstruct theoretical

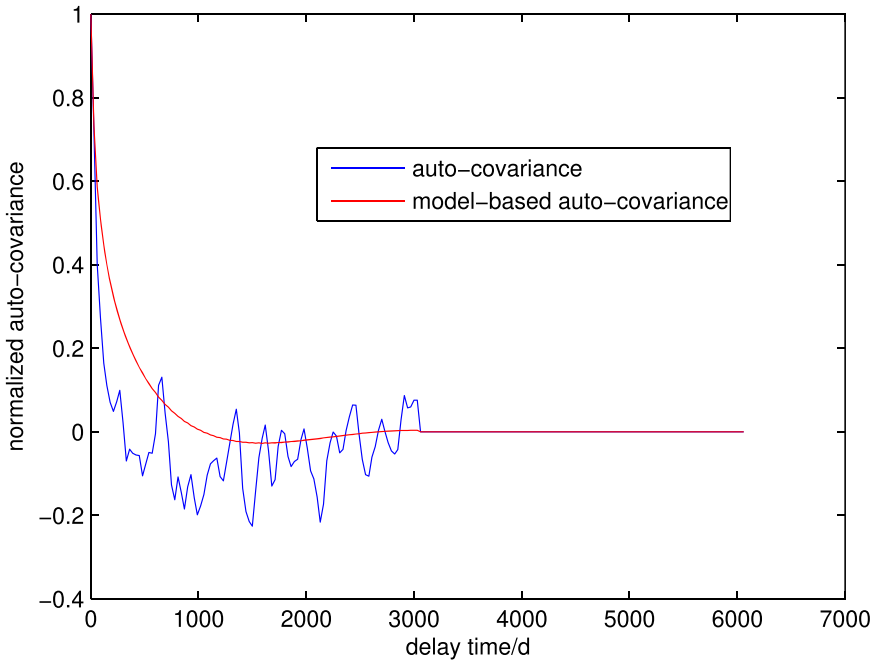

Figure 5. Normalized auto-covariance function of J0751+1807. The blue curve is derived from the auto-power spectrum of the residuals with respect to TAI. The red curve is derived from the auto-power spectrum based on a power-law model. The blue curve converges to the red one.

cross-power spectrum of each pulsar pair, and then derive the cross-covariance function for each pulsar pair by integrating Equation (8) using the reconstructed theoretical cross-power spectrum. The cross-covariance function is normalized. For the data set of ten pulsars, one have 45 independent pairs and their respective normalized cross-covariance functions. Finally we obtain average cross-covariance function representing more correctly the clock signal covariance by averaging 45 independent cross-covariance functions. Figure 6 shows the normalized average cross-covariance function based on model (the red curve), and the blue one is derived directly by the cross-power spectra of 45 pulsar pairs. The blue curve converges to the red one for the high frequency covariance.

(3) Signal realization in residuals by model

Residuals obtained by moving average and linear interpolation are basic observational results for each pulsar. These residuals still contain significant high frequency noise. Since auto-covariance function for each pulsar are based on its auto-power spectral power-law model, for consistency, the same auto-power spectral model should be used for signal realization in the residuals. We use signals in the residuals realized by the auto-power spectral model as input of the improved Wiener filtration algorithm. For example the residuals (blue line) and signal realization (red line) in the residuals by the power-law model for J1713+0747 are respectively shown in Figure 7.

We point that for our data set with respect to TAI of sample interval 30 days and 203 data points of each pulsar (see Section 2), power-law model fitting is based on power spectra of 50 consecutive low frequency components (corresponding to frequencies lower than $1/0.3$ yr) of the full spectrum both for auto-power spectrum and cross-power spectrum. Then auto-covariance function and cross-covariance function based on model parameters are respectively derived. The same power-law model parameters of auto-power spectrum are also used to signal realization in residuals for each pulsar. Usually the same low frequency components as power-law model fitting are used for calculating covariance function and signal realization in residuals. Sometimes we perhaps want to get a smoother ensemble pulsar timescale to compare with atomic clock, we can use power-law model parameters already fitted and lower frequency components to calculate auto- and cross-covariance function and signal realization in residuals (see Section 4.3).

The number of low frequency components of a power spectrum used for power-law model fitting relates to length of the vector $\boldsymbol{r}_I$ and sample interval of residuals. It is also helpful to reference to property of spectrum of the clock signal concerned, because our purpose is to extract clock signal. From the red curve in Figure 3, we estimate that 50 consecutive low frequency components of power spectrum for the TT(BIPM2015)−TAI can correctly represent clock signal we concerned. If spectral form of clock signal is not known, we can make a guess as closely as possible, or try calculating ensemble pulsar timescale based on power-law model fitting using different number of low frequency components close to the half of effective Fourier frequency components of a full power spectrum, and then select the best result. Fortunately the

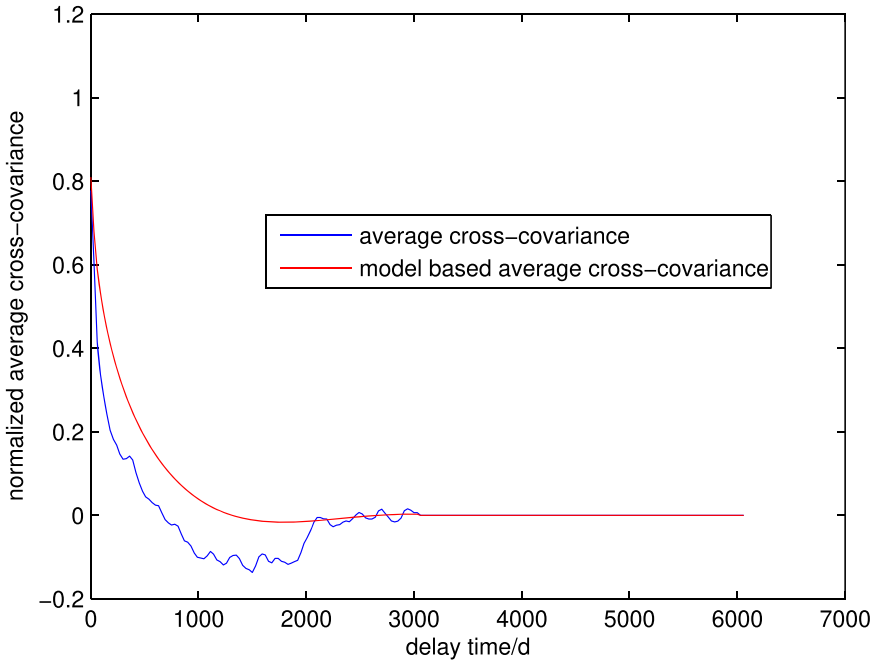

Figure 6. Normalized average cross-covariance function of 45 pulsar pairs in the data set with respect to TAI for ten pulsars. Blue curve is derived from cross-power spectra of pulsar pairs. Red curve is derived from cross-power spectra based on a power-law model of pulsar pairs. The blue curve is converged to the red curve.

final result is not strongly sensitive to small changes in the number of low frequency components used. For example when we calculate an ensemble pulsar timescale EPT−TT (BIPM2015), 40 consecutive low frequency components are used to fit a power-law model of auto- and cross-power spectrum.

4.2. Results

Following the description in Section 4.1, we derived average cross-covariance function based on the cross-power spectral power-law model and selected number of lower frequency components, this is considered as the covariance function of clock signal wanted. From the covariance function of clock signal we form covariance matrix $\boldsymbol{Q}_{\rm clk}$ of clock signal. Similarly an auto-covariance function is derived and auto-covariance matrix $\boldsymbol{Q}_{{\rm auto},I}$ is formed for the pulsar I. The realized residuals based on its auto-power spectral model and the same number of low frequency components as that used for calculating auto- and cross-covariance functions for the pulsar I are denoted as $\boldsymbol{r}_{s,I}$. According to Equation (2), the optimal estimate of signal for ensemble pulsar timescale can be written as

$$\hat{\boldsymbol{S}}_{\rm clk} = \boldsymbol{Q}_{\rm clk}\sum_{I=1}^{n}(w_I\boldsymbol{Q}^{-1}_{{\rm auto},I}\boldsymbol{r}_{s,I}), \tag{9}$$

where w_I is the normalized weight of pulsar I. Assuming $s_I = \boldsymbol{Q}^{-1}_{{\rm auto},I}\boldsymbol{r}_{s,I}$, σ_I is the rms of s_I, weight of the pulsar I is σ_I^{-2} and then normalized. Using the data set with respect to TAI for ten millisecond pulsars given in Section 2, we derived an ensemble pulsar timescale EPT−TAI and show it as the blue curve with error bars in Figure 8. The region of 1σ one-sided error is from 110 to 518 ns and with mean value of 310 ns for all the data points of the EPT−TAI. A description on method of uncertainty estimation of ensemble pulsar timescale data points is given in the Appendix. In Figure 8 the atomic timescale TT(BIPM2015)−TAI is shown as the red curve. We see that the EPT−TAI shows a similar trend as TT(BIPM2015) −TAI, and high frequency noise of EPT−TAI is much smaller than EPT1−TAI in Figure 2.

Using the same algorithm as that for EPT−TAI, we also calculated an ensemble pulsar timescale EPT−TT(BIPM2015) with the data set respect to TT(BIPM2015) given in Section 2. For EPT−TT(BIPM2015) calculation 40 Fourier lower frequency components of spectrum is used.

When we calculate EPT1−TAI and EPT−TAI, their normalized weight for each pulsar is given respectively in Table 1. The weight of each pulsar is very different. Pulsars J0437-4715 and J1713+0747 always take larger weights, The sum of normalized weight for these two pulsars is about 0.8 for both EPT1−TAI and EPT−TAI cases. The third one with larger weight is pulsar J1744-1134. We note that these three pulsars have lower rms of residuals and their number of TOAs available is relatively more. Weight of each pulsar for constructing EPT−TT(BIPM2015) is same as that for EPT−TAI.

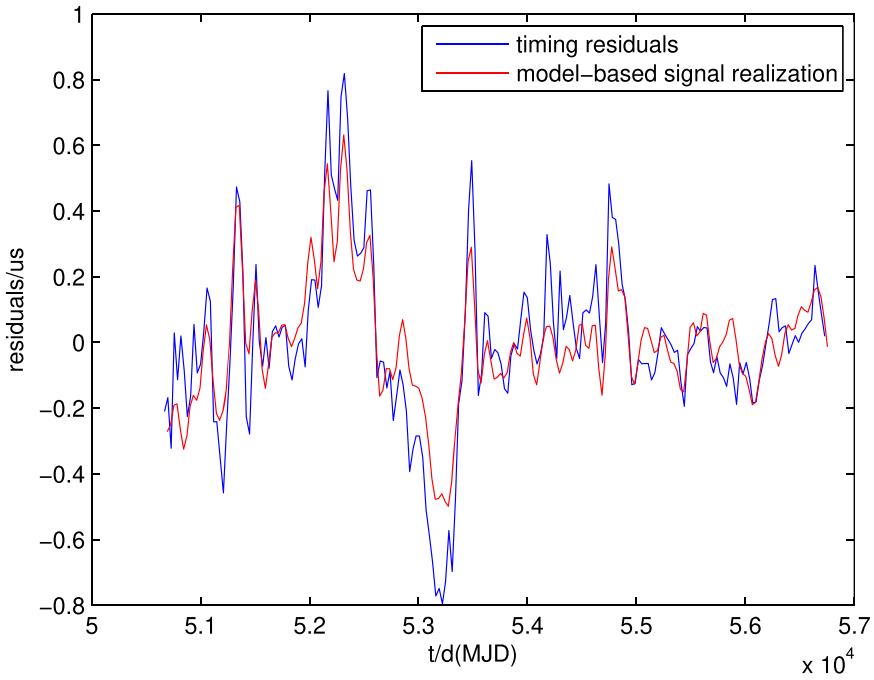

Figure 7. Residuals with respect to TAI from moving average and interpolation (blue curve) and signal realization in the residuals with Fourier frequency components lower than $1/0.3$ yr based on the auto-power spectral power-law model for pulsar J1713+0747 (red curve).

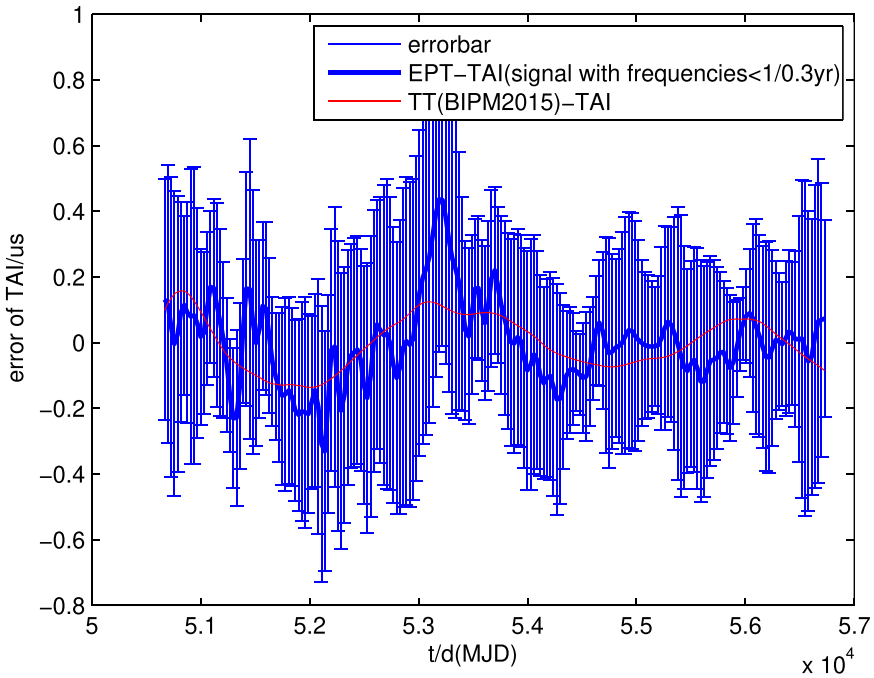

Figure 8. Ensemble pulsar timescale EPT−TAI (blue curve with error bar) derived by Wiener filtration based on a power-law model. For EPT−TAI calculation 50 Fourier low frequency components of spectrum (corresponding to frequencies $<1/0.3$ yr) are used for the power-law model fitting, covariance function computation and signal realization in pulsar residuals. The signal of TT(BIPM2015)−TAI is shown by the red curve.

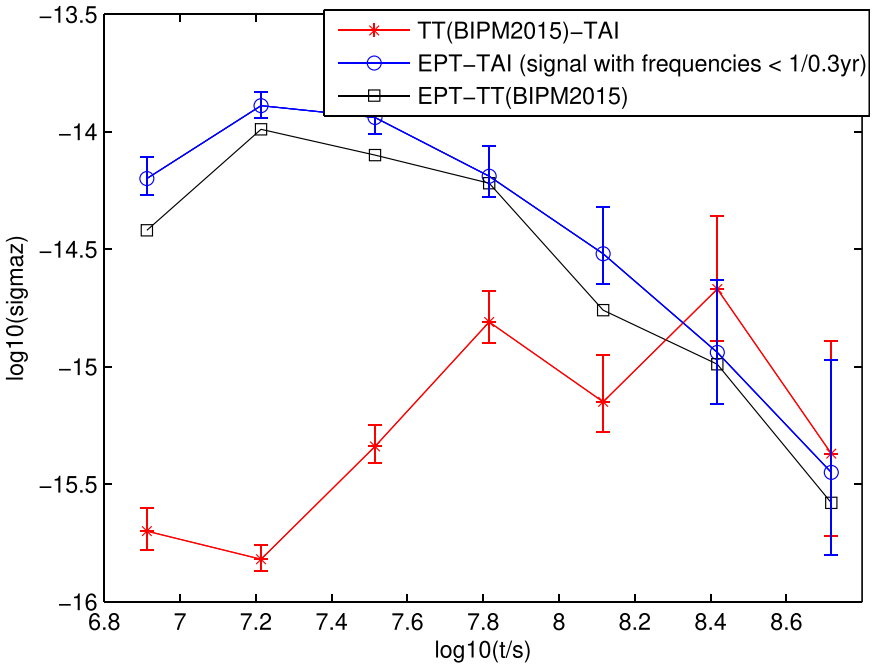

Figure 9. Comparison of σ_z for timescales. It is clear that some red noise of TT(BIPM2015)−TAI is presented, but there is no red noise observed for EPT−TAI and EPT−TT(BIPM2015). σ_z for EPT−TT(BIPM2015) is similar to that for EPT−TAI but with slightly lower values. Error-bars of black curve are omitted for clarity since they are similar to those of the blue one.

4.3. Analysis of Fractional Frequency Stability of Time Scales

We calculated σ_z (Matsakis et al. 1997) of the EPT−TAI derived above and showed it as blue line in Figure 9. For comparison, σ_z of the atomic time TT(BIPM2015)-TAI is shown as the red line. The σ_z curve of EPT−TT(BIPM2015) is also shown as the black one in Figure 9. Conventional Fourier techniques necessarily fail in the presence of steep power-law spectra because of spectral leakage between frequency bins. In contrast, the effective "filters" corresponding to the σ_z technique have steep cutoffs on their low frequency sides and hence are ideal for analyzing red noise (Matsakis et al. 1997). In Figure 9, the $\log 10(\sigma_z)$ corresponding to $t = 10^{6.9}$ s($t = 90$ days) biased down for both EPT−TAI and EPT−TT(BIPM2015). This phenomenon may relate to moving average of original timing residuals. The total shape of σ_z curves for both ensemble pulsar timescales EPT−TAI and EPT−TT(BIPM2015) go down as time increases, while σ_z curve of atomic timescale TT(BIPM2015) −TAI goes up. It is clear that the atomic timescale TT(BIPM2015)−TAI shows red noise for longer time intervals. Contrarily the EPT−TAI does not show red noise even for about 16 yr time interval. In this case, fractional frequency stability of the EPT-TAI for $t = 10^{8.4}$ s($t = 8$ yr) and longer intervals is slightly better than that of TT(BIPM2015)−TAI. If it is further certified by more research works on the ensemble pulsar timescale that the long term fractional stability of pulsar timescale is better than the atomic timescale, we may improve the long term stability of the TT(BIPM2015)−TAI by the ensemble pulsar timescale. Figure 9 shows that fractional frequency stability for short times for TT(BIPM2015)−TAI is better than the ensemble pulsar timescale. From Figure 8 we also see that the curve of TT(BIPM2015)−TAI is much smoothing compared to the curve of EPT−TAI. Obviously EPT−TAI contains some level high frequency noise.

In order to test σ_z of pulsar timescales with different smoothing levels, we tried deriving a smoother ensemble pulsar timescale through reducing number of Fourier lower frequency components of spectra used for covariance function computation and signal realization in pulsar residuals but keeping the power-law model fitting process unchanged. In Figure 10 we show σ_z results of two ensemble pulsar timescales with different smoothing levels. Compared with blue curve σ_z the black curve for short time intervals ($t < 2$ yr) is improved but σ_z for $t > 2$ yr is almost not changed.

5. Discussion and Conclusion

There are different algorithms for ensemble pulsar timescales (Zhong & Yang 2007; Rodin 2008; Hobbs et al. 2020). The algorithm of Wiener filtration is perhaps operational simpler one. Comparison between results based on different algorithms

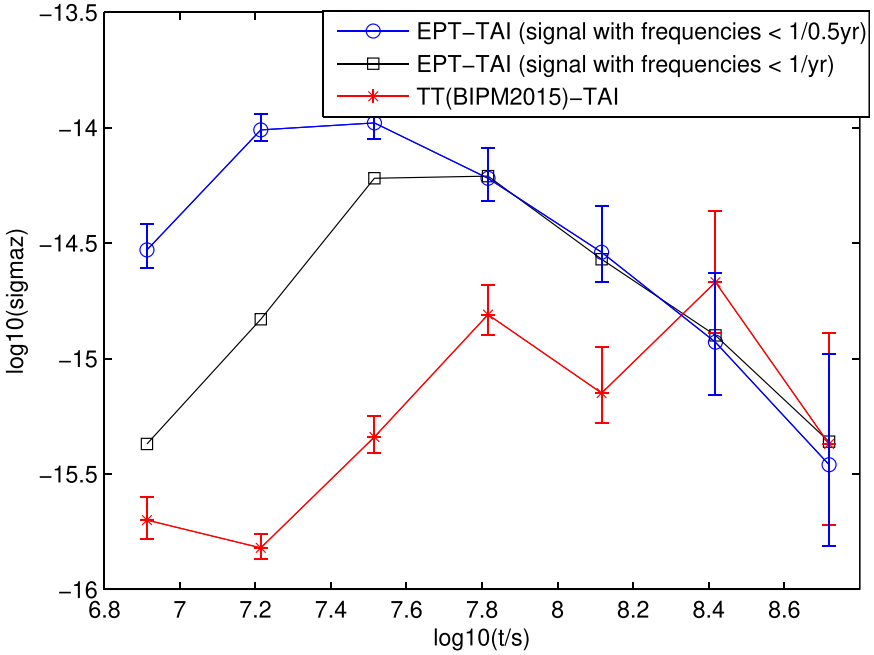

Figure 10. σ_z of ensemble pulsar timescales with different smoothing levels. A smoother pulsar timescale is derived by improved Wiener filtration using lesser number of Fourier lower frequency components of power spectra except power-law model parameter fitting unchanged. The fractional frequency stability of the black curve for short time intervals is improved than that of the blue one, stability for $t > 10^{7.8}$ s($t > 2$ yr) is almost same in any case. σ_z for atomic timescale TT(BIPM2015)−TAI is shown by the red curve.

is necessary for developing an ensemble pulsar timescale. Wiener filtration requires that TOA data samples for all the pulsars used to construct an ensemble timescale have the regular time distribution over the same time span. TOA data processing before carrying constructing the ensemble pulsar timescale is necessarily important. The purpose of TOA data processing is to correctly derive post-fit timing residuals which keep clock signals concerned for each pulsar. In order to do this, any systematic errors in the selected data related to observational system and DM variations must be removed. TOA measurement errors must be calibrated and red noise that may be present should be estimated. Then a fitting process using Tempo2 package is carried out to get post-fit residuals. Because of irregular sample of original TOA data, averaging and interpolating of post-fit residuals is required to get uniformly distributed post-fit residual samples for each pulsar.

In order to more effectively extract clock signals buried in timing noise, we developed a Wiener filtration algorithm based on power-law model of pulsar power spectrum. Using ten millisecond pulsar timing data with about 16 yr long from IPTA second data release, employing the Wiener filtration algorithm we developed, an ensemble pulsar timescale EPT−TAI is calculated. Results show that the EPT−TAI correctly detected clock signal TT(BIPM2015)−TAI. Fractional frequency stability σ_z analysis shows that EPT −TAI does not indicate red noise for 16 yr time interval, and fractional frequency stability for 8 yr and longer intervals is slightly better than that of TT(BIPM2015)−TAI. This result needs to be further verified by more research works. Stability for short time intervals of TT(BIPM2015)−TAI is better than EPT−TAI, but TT(BIPM2015)−TAI shows red noise for longer time intervals.

Fractional frequency stability of ensemble pulsar timescale on short time intervals is worse compared to atomic timescale TT−TAI, mainly because of larger measurement noise of TOAs. Fractional stability on short times of ensemble pulsar timescale can be improved by further filtering out high frequency noise. Reducing measurement errors of TOAs, for example TOA measurement errors by FAST telescope reduced to 50 ns, will lead to improvement of fractional stability on short time intervals of ensemble pulsar timescale in the future.

Acknowledgments

This work is supported from the National Natural Science Foundation of China (Grant Nos. 42030105, 11973046, U1831130, and 91736207) and the Ministry of Science and Technology of China (Grant No. 2020SKA0120103).

Appendix
Method of Error Estimation of Ensemble Pulsar Timescale for Improved Wiener Filtration

For pulsar I, its clock signal estimation is computed by

$$\hat{\boldsymbol{S}}_{\mathrm{clk},I} = \boldsymbol{Q}_{\mathrm{clk}} \boldsymbol{Q}^{-1}_{\mathrm{auto},I} \boldsymbol{r}_{s,I}. \tag{A1}$$

In Equation (A1), $\boldsymbol{Q}_{\mathrm{clk}}$ is covariance matrix for clock signal, $\boldsymbol{Q}_{\mathrm{auto},I}$ is auto-covariance matrix for pulsar I and $\boldsymbol{r}_{s,I}$ is realized residual vector for pulsar I by the model. Covariance of $\hat{S}_{\mathrm{clk},I}$ can be estimated by referencing Equation (42) of Lee et al. (2014). An ensemble pulsar timescale using data of n pulsars is derived by equation

$$\hat{\boldsymbol{S}}_{\mathrm{clk}} = \boldsymbol{Q}_{\mathrm{clk}} \sum_{I=1}^{n} (w_I \boldsymbol{Q}^{-1}_{\mathrm{auto},I} \boldsymbol{r}_{s,I}). \tag{A2}$$

In Equation (A2), w_I indicates the normalized weight for pulsar I. Error estimation for waveform of an ensemble pulsar timescale derived with Equation (A2) is computed by equation

$$\boldsymbol{\sigma}_{\mathrm{clk},i} = \left[\left(\sum_{I=1}^{n} w_I \hat{\boldsymbol{S}}^2_{\mathrm{clk},I,i} \right) - \hat{\boldsymbol{S}}^2_{\mathrm{clk},i} \right]^{1/2}, \tag{A3}$$

where subscript i represents the ith element of corresponding vector.

References

Caballero, R. N., Lee, K. J., Lentati, L., et al. 2016, MNRAS, 457, 4421
Coles, W., Hobbs, G., Champion, J. D., et al. 2011, MNRAS, 418, 561
Edwards, R. T., Hobbs, G., & Manchester, R. N. 2006, MNRAS, 372, 1549
Guinot, B. 1988, A&A, 192, 370
Hobbs, G. 2012, IAUS, 291, 165
Hobbs, G., Archibald, A., Arzoumanian, Z., et al. 2010, CQGra, 27, 084013
Hobbs, G., Coles, W., Manchester, R. N., et al. 2012, MNRAS, 427, 2780
Hobbs, G., Guo, L., Caballero, R. N., et al. 2020, MNRAS, 491, 5951
Keith, M. J., Coles, W., Shannon, R. M., et al. 2013, MNRAS, 429, 2161
Lee, K. J., Bassa, C. G., Janssen, G. H., et al. 2014, MNRAS, 441, 2831
Lentati, L., Alexander, P., & Hobson, M. P. 2013, PhRvD, 87, 104021
Lentati, L., Alexander, P., Hobson, M. P., et al. 2014, MNRAS, 437, 3004
Lentati, L., Taylor, S. R., Mingarelli, C. M. F., et al. 2015, MNRAS, 453, 2576
Manchester, D., Verbiest, J. P. W., Sarkissian, J., et al. 2007, ATNF proposal id P456 Semester, October
Manchester, R. N. 2011, in AIP Conf. Proc. 1357 (Sardinia, Italy) (Melville, NY: AIP), 65
Matsakis, D. N., TaylorJ, H., & Eubanks, T. M. 1997, A&A, 326, 924
Perera, B. B. P., Decesar, M. E., Demorest, P. B., et al. 2019, MNRAS, 490, 4666
Petit, G., & Tavella, P. 1996, A&A, 308, 290
Rodin, A. E. 2008, MNRAS, 387, 1583
van Haasteren, R., & Levin, Y. 2009, MNRAS, 395, 1005
van Haasteren, R., Levin, Y., & McDonald, P. 2013, MNRAS, 428, 1147
Verbiest, J. P. W., Lentati, L., Hobbs, G., et al. 2016, MNRAS, 458, 1267
Zhong, C. X., & Yang, T. G. 2007, AcPSn, 10, 6157, in Chinese